NUMERICAL STUDY OF TURBULENT MAGNETOHYDRODYNAMIC CONVECTION OF MOLTEN SODIUM WITH VARIABLE PROPERTIES IN A SQUARE CAVITY

by

Mohsen PIRMOHAMMADI
Mechanical Engineering Department, Pardis Branch, Islamic Azad University, Tehran, Iran

Original scientific paper
https://doi.org/10.2298/TSCI171115083P

In this study, the finite volume method is used to simulate the turbulent natural convection in a square partitioned cavity. In this paper a fluid-flow with Pr = 0.01 and Ra = 10^6 and 10^7 in the presence of a magnetic field is investigated. The fluid properties are function of temperature. A parametric study is carried out using following parameters: non-dimensional different partition position from 0.2 to 0.6, non-dimensional different partition height from 0.1 to 0.4, and different Hartmann numbers from 0 to 200. It is found that Nusselt number is a decreasing function of partition height, H_p, and Hartmann number and the non-dimensional position of partitions, D_p, affects on streamlines and isotherms. It is observed that at Ra = 10^6 and D_p = 0.6 the Nusselt number is maximum and as Hartmann number increases the Nusselt number tends to a constant number. Also at Ra = 10^7 and D_p = 0.4 the variation of mean Nusselt number for different partition heights is more different than the other cases. Also the Nusselt number at H_p = 0.4 is nearly half for D_p = 0.4 in comparison with the other cases.

Key words: *numerical study, MHD convection, molten sodium, square cavity*

Introduction

The natural convection of an electrically conducting fluid in an enclosure in the presence of a magnetic field has been thoroughly studied by several researchers in the laminar flow $\mathrm{Ra} < 10^6$ [1-6]. Comparatively little attention has been paid to the turbulent flow, $\mathrm{Ra} \geq 10^6$, which is also of interest for many industrial processes.

A numerical 2-D study is carried out on the laminar and turbulent natural convection of sodium in a square enclosure heated from one vertical wall and cooled from an opposing vertical wall was studied by Jalil and Al-Tae'y [7]. They showed that the effect of a non-uniform magnetic field differs from that of a uniform magnetic field. The flow profile changes dramatically with external magnetic strength and direction, but this change in flow region depends on the distribution of magnetic field strength along magnetic pole faces.

Kakarantzas *et al.* [8] investigated laminar and turbulent regimes of a liquid metal flow in a vertical annulus under constant horizontal magnetic field numerically. They have considered that flow is driven by using the volumetric heating and temperature difference between the two cylindrical walls. Their results illustrated that when the magnetic field increases, the

Author's e-mail: pirmohamadi@pardisiau.ac.ir

flow becomes laminar. Also, they observed that the magnetic field causes the loss of axisymmetry of flow.

Liu *et al.* [9] adopted the large-eddy-simulation technique with the dynamic subgrid scale model for body-fitted grids to investigate turbulent melt convection in an ellipsoidal crucible. Numerical comparisons were carried out for three configurations: without magnetic field, with a transverse magnetic field, and with a cusp-shaped magnetic field.

Direct numerical simulation results of MHD liquid metal flow between two vertical coaxial cylinders under the effect of internal heating and a horizontal magnetic field was presented by Kakarantzas *et al.* [10]. They showed that the heat sources create bi-cellular flow patterns as the maximum temperature in inside the fluid bulk. The flow is azimuthally asymmetric due to the Hartmann and Robert layers formed on the walls normal and parallel to the magnetic field, respectively.

Zhang and Zikanov [11] studied 2-D turbulent convection in a toroidal duct of a liquid metal blanket of a fusion reactor. They found the turbulence results in stronger mixing and more uniform distribution of wall heat flux, indicating promising potential of this concept of the blanket.

Sajjadi and Kefayati [12] investigated MHD turbulent and laminar natural convection in a square cavity utilizing lattice Boltzmann method (LBM). The main aim of this study is to identify the ability of the LBM for solving turbulent MHD natural convection with a simple method. The MHD natural convection in a square cavity which was filled with a fluid with Pr = 6.2 for different flow regimes with various Rayleigh numbers were studied.

Natural convection in a differentially laterally heated vertical cylindrical reactor was numerically studied using ANSYS FLUENT in a 2-D axisymmetric configuration by Enayati *et al*. [13]. The main goal of this paper was to define and study the boundaries of the transitional flow regime leading to turbulent flow for this thermal configuration. Seven cases for a range of Rayleigh numbers from 750 to 8.8×10^8 were studied by using the FLUENT k-ω SST turbulent model.

This paper is devoted to the study of turbulent convection heat transfer Ra = 10^6 and Ra = 10^7 in molten sodium under the influence of uniform magnetic field. The k-ε turbulence model was used. The effect of a magnetic field and partition height and its position on average Nusselt number, isotherms and streamlines is investigated.

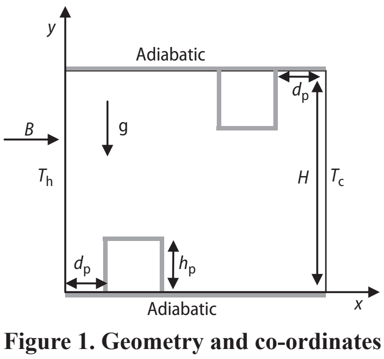

Figure 1. Geometry and co-ordinates of enclosure configuration with magnetic effect

Governing equations

The geometry of the present problem is shown in fig. 1. It consists of a 2-D cavity with height, H. The temperatures of the two sidewalls of the cavity are maintained at T_h and T_c, where T_c has been considered as the reference condition. The horizontal walls are assumed to be insulated, non-conducting, and impermeable to mass transfer.

Magnetic field of strength, B_0, is applied longitudinally. The top and bottom walls are insulated and the fluid is isothermally heated and cooled by the left and right walls at uniform temperatures of T_h and T_c, respectively.

Dimensionless variables in the analysis are defined:

$$X=\frac{x}{H},\quad Y=\frac{y}{H},\quad H_p=\frac{h_p}{H},\quad D_p=\frac{d_p}{H},\quad U=\frac{uH}{\alpha},\quad V=\frac{vH}{\alpha},\quad P=\frac{pH^2}{\rho\alpha^2},$$
$$\theta=\frac{T-T_c}{T_h-T_c},\quad \varepsilon^*=\frac{\varepsilon H^4}{\alpha^3},\quad \sigma^*=\frac{\sigma}{\sigma_r},\quad \mu_{eff}^*=\frac{\mu_{eff}}{\mu_r},\quad \mu_t^*=\frac{\mu_t}{\mu_r},\quad \Gamma_{\text{eff},\kappa}^*=\frac{\Gamma_{eff,\kappa}}{\mu_r},\tag{1}$$
$$\kappa^*=\frac{\kappa H^2}{\alpha_r^2},\quad \Gamma_{\text{eff},\varepsilon}^*=\frac{\Gamma_{\text{eff},\varepsilon}}{\mu_r},\quad \Gamma_{\text{eff},t}^*=\frac{\Gamma_{\text{eff},t}}{k_r}$$

where u and v are the velocity components, p – the pressure, T – the temperature, α – the thermal diffusivity, ρ – the density, $\mu_{\text{eff}}=\mu+\mu_t$, $\Gamma_{\text{eff,t}}=k_r+\mu_t cp_r/\sigma_t$, $\Gamma_{\text{eff},\kappa}=\mu_r+\mu_t/\sigma_\kappa$ and, $\Gamma_{\text{eff},\varepsilon}=\mu_r+\mu_t/\sigma_\varepsilon$, μ_t – the turbulent viscosity that related to k and ε [14].

According to the aforementioned dimensionless variables, the governing equations in this study are based on the conservation laws of mass, linear momentum, energy and magnetic induction are given in dimensionless form:

$$\frac{\partial U}{\partial X}+\frac{\partial V}{\partial Y}=0\tag{2}$$

$$U\frac{\partial U}{\partial X}+V\frac{\partial U}{\partial Y}=-\frac{\partial P}{\partial X}+2\Pr\frac{\partial}{\partial X}\left(\mu_{\text{eff}}^*\frac{\partial U}{\partial X}\right)+\Pr\frac{\partial}{\partial Y}\left(\mu_{\text{eff}}^*\frac{\partial U}{\partial Y}+\mu_{\text{eff}}^*\frac{\partial V}{\partial X}\right)\tag{3}$$

$$U\frac{\partial V}{\partial X}+V\frac{\partial V}{\partial Y}=-\frac{\partial P}{\partial Y}+\Pr\frac{\partial}{\partial X}\left(\mu_{\text{eff}}^*\frac{\partial V}{\partial X}+\mu_{\text{eff}}^*\frac{\partial U}{\partial Y}\right)+2\Pr\frac{\partial}{\partial Y}\left(\mu_{\text{eff}}^*\frac{\partial V}{\partial Y}\right)+\text{Ra}\Pr\theta-\text{Ha}^2\Pr V\tag{4}$$

$$\frac{\partial(c_p^*U\theta)}{\partial X}+\frac{\partial(c_p^*V\theta)}{\partial Y}=\frac{\partial}{\partial X}\left(\Gamma_{\text{eff},t}^*\frac{\partial\theta}{\partial X}\right)+\frac{\partial}{\partial Y}\left(\Gamma_{\text{eff},t}^*\frac{\partial\theta}{\partial Y}\right)\tag{5}$$

$$\frac{\partial}{\partial X}(U\kappa^*)+\frac{\partial}{\partial Y}(V^*\kappa^*)=\Pr\frac{\partial}{\partial x}\left(\Gamma^*{}_{\text{eff},\kappa}\frac{\partial\kappa^*}{\partial X}\right)+\Pr\frac{\partial}{\partial Y}\left(\Gamma^*{}_{\text{eff},\kappa}\frac{\partial\kappa^*}{\partial y}\right)+P_\kappa^*+G_\kappa^*-\varepsilon^*$$
$$P_\kappa^*=2\Pr\mu_t^*\left[\left(\frac{\partial U}{\partial Y}\right)^2+\left(\frac{\partial V}{\partial Y}\right)^2+\left(\frac{\partial U}{\partial Y}+\frac{\partial V}{\partial X}\right)^2\right],\quad G_\kappa^*=-\frac{\mu_t^*}{\sigma_t}\text{Ra}\Pr^2\frac{\partial\theta}{\partial Y}-\varepsilon^*\tag{6}$$

$$\frac{\partial}{\partial X}(U\varepsilon^*)+\frac{\partial}{\partial Y}(V\varepsilon^*)=\frac{\partial}{\partial X}\left(\Gamma_{\text{eff},\varepsilon}^*\frac{\partial\varepsilon^*}{\partial X}\right)+\frac{\partial}{\partial Y}\left(\Gamma_{\text{eff},\varepsilon}^*\frac{\partial\varepsilon^*}{\partial Y}\right)+P_\varepsilon^*+G_\varepsilon^*-D_\varepsilon^*$$
$$P_\varepsilon^*=C_1\left\{2\mu_t^*\left[\left(\frac{\partial U}{\partial Y}\right)^2+\left(\frac{\partial V}{\partial Y}\right)^2+\left(\frac{\partial U}{\partial Y}+\frac{\partial V}{\partial X}\right)^2\right]\right\}\Pr\frac{\varepsilon^*}{\kappa^*},\tag{7}$$
$$G_\varepsilon^*=C_1C_3\,\text{Ra}\Pr^2\left(\frac{\mu_{\text{eff}}^*}{\sigma_t}\frac{\partial\theta}{\partial Y}\right)\frac{\varepsilon^*}{\kappa^*},\quad D_\varepsilon^*=c_2\frac{\varepsilon^{*2}}{\kappa^*}$$

where Pr, Ra, and Ha are the Prandtl, Rayleigh, and Hartmann numbers, respectively, are defined:

$$\Pr=\frac{\nu}{\alpha},\quad \text{Ra}=\frac{g\beta(T_\text{h}-T_\text{c})H^3}{\alpha\nu},\quad \text{Ha}=B_0H\sqrt{\frac{\sigma}{\rho\nu}}\tag{8}$$

where g is the gravitational acceleration, ν – the kinematic viscosity, β – the coefficient of thermal expansion, B_0 – the magnitude of magnetic field, and σ – the electrical conductivity. It is noted that $\mathrm{Ha}^2 \mathrm{Pr} V$ in eq. (4) is achieved by simplifying the Lorentz force term ($\vec{J} \times \vec{B}$) using constant magnetic field. The magnetic Reynolds number, Re_m, is very small in most of the engineering applications so that the magnetic field, $\vec{B}$, is unchanged by the flow [15, 16].

Also, the used constants in above equations are presented in tab. 1 as follows:

Table 1. Constants used in k-ε model

C_1	C_2	C_3	C_μ	σ_k	σ_t	σ_ε
1.44	1.92	tanh(|v/u|)	0.09	1.0	1.0	1.3

In order to compare total heat transfer rate, Nusselt number is used. The local and average Nusselt numbers are defined:

$$\mathrm{Nu}_y = -\left.\frac{\partial \theta}{\partial X}\right|_{X=0}, \quad \overline{\mathrm{Nu}} = \int_0^1 \mathrm{Nu}_y \mathrm{d}Y \tag{9}$$

Boundary conditions are:

$$U \text{ and } V = 0 \text{ at all walls } (X = 0, X = 1, Y = 0, Y = 1) \tag{10}$$

$$\theta(0,Y) = 1, \quad \theta(1,Y) = 0, \quad \left.\frac{\partial \theta}{\partial Y}\right|_{Y=0} = 0, \quad \left.\frac{\partial \theta}{\partial Y}\right|_{Y=1} = 0 \tag{11}$$

On the partitions:

$$\frac{\partial \theta}{\partial X} = 0, \quad \frac{\partial \theta}{\partial Y} = 0 \tag{12}$$

Also, wall functions are used for turbulent parameters [17]:

$$y^+ = \rho \frac{C_\mu^{1/4} k'^{1/2}}{\mu} y_p, \quad k' = 0.41 \tag{13}$$

$$T^+ = -\frac{\rho \kappa'^{1/2} (c_\mu)^{1/4}}{\sigma_t \left\{ \left[\frac{1}{\kappa'} \ln(E y^+) \right] + CT \right\}},$$

$$CT = 9.24 \left[1 + 0.28 \exp\left(-0.007 \frac{\mathrm{Pr}}{\sigma_t} \right) \right] \left[\left(\frac{\mathrm{Pr}}{\sigma_t} \right)^{1/4} - 1 \right] \tag{14}$$

Numerical method

The governing equations associated with the boundary conditions are solved numerically, employing a finite volume method. In order to couple the velocity field and pressure in the momentum equations, the well-known SIMPLER-algorithm [18] is adopted. The hybrid-scheme, which is a combination of the central difference scheme and the upwind scheme, is used to discretize the convection terms. A staggered grid system [18], in which the velocity components are stored midway between the scalar storage locations, is used. The solution of the fully coupled discretized equations is obtained iteratively using the TDMA method [18]. Special consideration for the number of grid points is given so that the narrow Hartmann boundary layers are adequately covered at the boundaries. To check the grid independency, the simulations were carried on for cell numbers ranging from 31×31 to 151×151 for Ra = 10^7 and Ha = 100. It was found that using the 121×121 mesh leads to the grid independent result. In tab. 2 the results of ψ_{max} and $\overline{\text{Nu}}$ at the hot wall are presented. As it can be seen, changing the grid from 101×101 to 121×121 will make approximately 0.1 percent difference in the mentioned results. According to the grid dependency analysis, all results presented from now on, are generated by 121×121 grid, fig. 2.

Table 2. Results of $\overline{\text{Nu}}$ for different mesh sizes (Ra = 107 and Ha = 100)

Mesh size	$\overline{\text{Nu}}$
51×51	102
61×61	3.227
91×91	3.199
101×101	3.187
121×121	3.183

Results and discussion

Validations

In order to check the accuracy of the numerical technique employed for the solution of the problem considered in the present study, it was validated by performing simulation for magneto-convection flow in a square enclosure with horizontal temperature gradient and in the presence of magnetic field which were reported by Jalil and Al-Tae'y [7]. Figure 3 plots the streamlines and isotherms for the present solution and the results published by Jalil for Ra = 10^{10}, Ha = 0 and Pr = 0.01.

In this comparison the properties of fluid were assumed to be constant and the induced magnetic field due to the motion of the electrically conducting fluid was neglected. It is observed that results show good agreement with the Jalil's work.

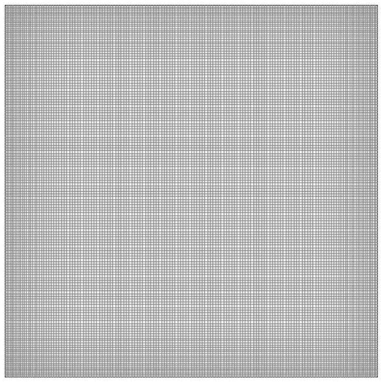

Figure 2. Grid distributions inside the domain

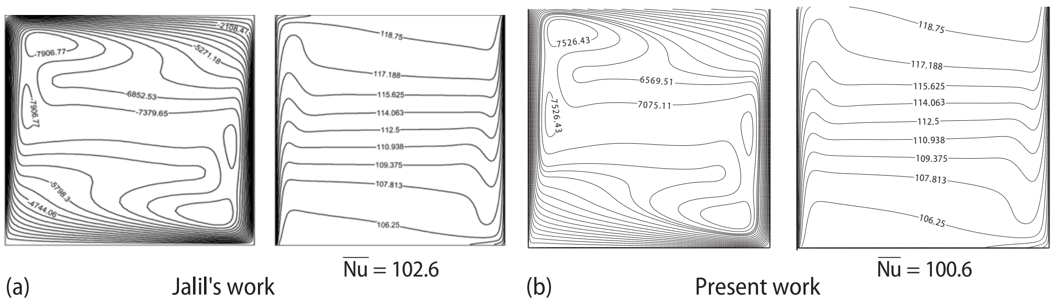

Figure 3. Streamlines and isotherms of natural convection in a square enclosure for Ra = 10^{10} and Ha = 0 (the fluid properties are constant)

Turbulent natural convection heat transfer of molten sodium inside a partitioned enclosure in the presence of magnetic field is investigated. The fluid properties are function of sodium temperature. The Rayleigh numbers 10^6 and 10^7, different Hartmann numbers, H_p = 0.1, 0.2, 0.3, 0.4, and D_p = 0.2, 0.4, 0.6 are considered.

Flow field and heat transfer for Ra = 10^6

For Ra = 10^6 and H = 0.124 m, the difference between temperature of hot wall and cold wall will be 16 °C and this causes the variation of fluid properties to be rather low.

Figure 4 presents the isotherms and streamlines for Ra = 106, $H_P = 0.2$, $D_P = 0.2$, and Hartmann numbers between 0 and 400. In fig. 4(a) it is shown that at Ha = 0 in addition to main flow two secondary vortices and also two counter clockwise vortexes on the partitions are formed. As Hartmann number increases the secondary vortices disappeared and concentration of streamlines near hot and cold wall disappeared but again at Ha = 400 the weak secondary vortices at center of enclosure are observed.

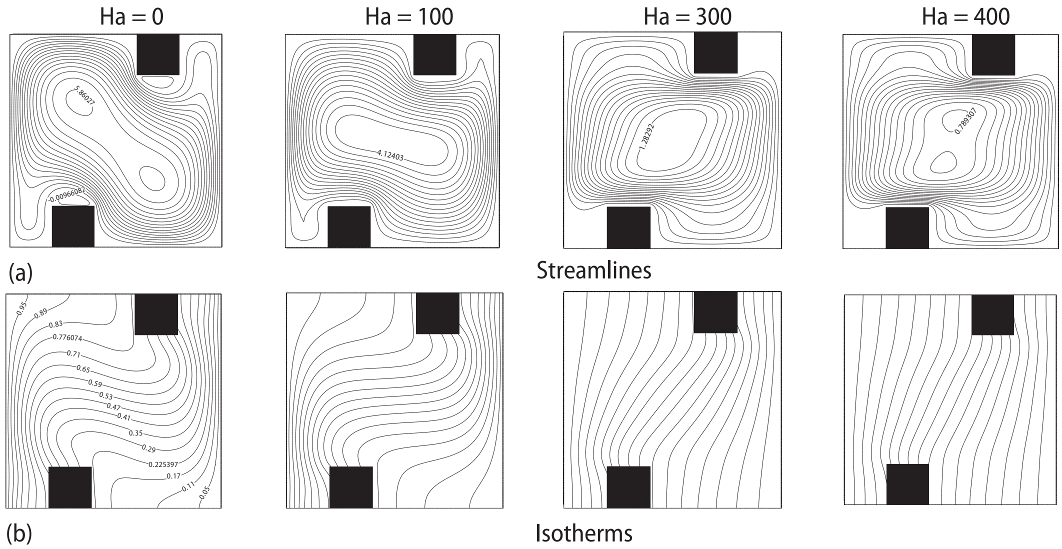

Figure 4. Streamlines (a) and isotherms (b) for $D_p = 0.2$, Ra = 10^6 and different Hartmann numbers

In fig. 4(b) it is seen that there is a temperature stratification between two partitions in the vertical direction and the isotherms in the center of the enclosure are restricted to the partitions. By applying magnetic field, the temperature stratification diminishes and as Hartmann number increases the temperature gradient becomes lower.

Figure 5 presents the streamline and isotherm plots for Rayleigh number 10^6, $H_P = 0.2$, $D_P = 0.4$, and Hartmann numbers between 0 and 400.

In fig. 5(a) it is shown that at Ha = 0 two counterclockwise vortices are formed behind the partitions. As Hartmann number increases near the left and right walls the Lorentz force is induced in opposite direction of the buoyancy force and causes the centerline of the main vortex rotates in counterclockwise. At high Hartmann number (Ha = 400) two secondary vortices are formed at the center of enclosure. It is evident from fig. 5(b) at Ha = 0 the isotherms between the partitions are skewed that indicates the convection is dominant in this region but by applying magnetic field and increasing the Hartmann number the isotherms will be vertical and heat transfer between two side walls is occurred by conduction.

Figure 6 presents the streamline and isotherm plots for $D_p = 0.6$.

In fig. 6(a) it is seen that when Ha = 0, the centerline of primary vortex is horizontal and secondary vortices are not formed inside the main flow but two large vortices behind the partitions appeare. It is evident from fig. 6(b) at low Hartmann numbers the concentration of isotherms near hot and cold walls for $D_p = 0.6$ is more than other cases and this means that the heat transfer in this case is the most.

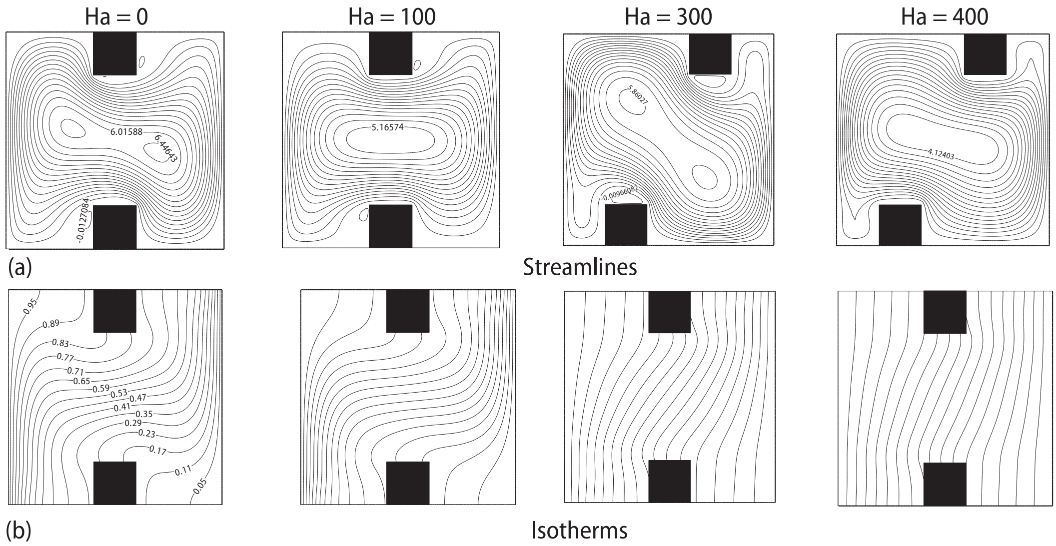

Figure 5. Streamlines (a) and isotherms (b) for D_p = 0.4, Ra = 10^6 and different Hartmann numbers

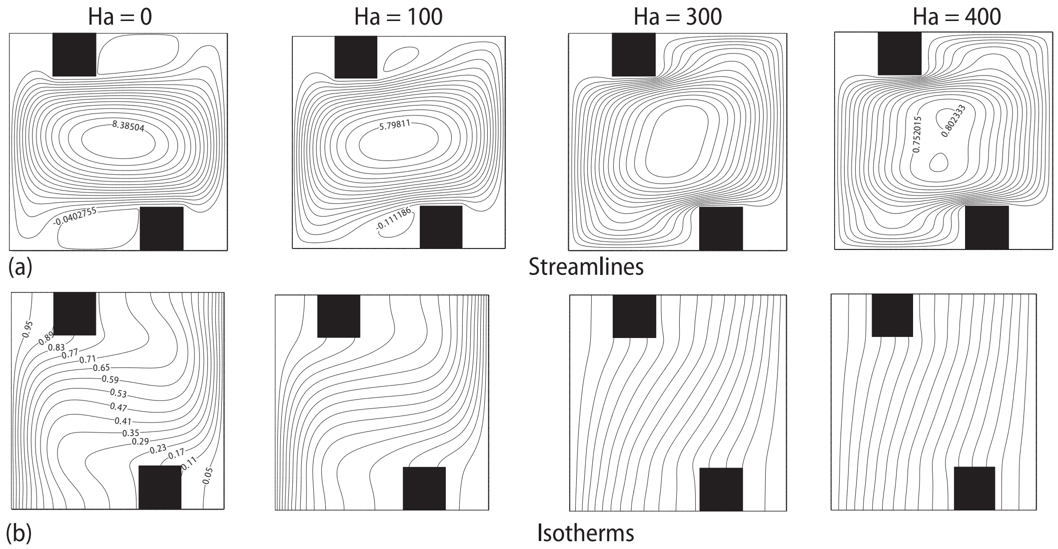

Figure 6. Streamlines (a) and isotherms (b) for D_p = 0.6, Ra = 10^6 and different Hartmann number

Figure 7 depicts the variation of the mean Nusselt number with Hartmann number versus several partition heights for D_p = 0.2, D_p = 0.4, D_p = 0.6, and Ra = 10^6. Generally, it is observed that as Hartmann number and partitions height increase the mean Nusselt number decreases. In low Hartmann numbers deviation between Nusselt numbers for different H_p is high and with increasing the magnetic field strength this deviation decreases. Also, it is seen that at D_p = 0.6 the Nusselt number is maximum and as Hartmann number increases the Nusselt number tends to a constant number.

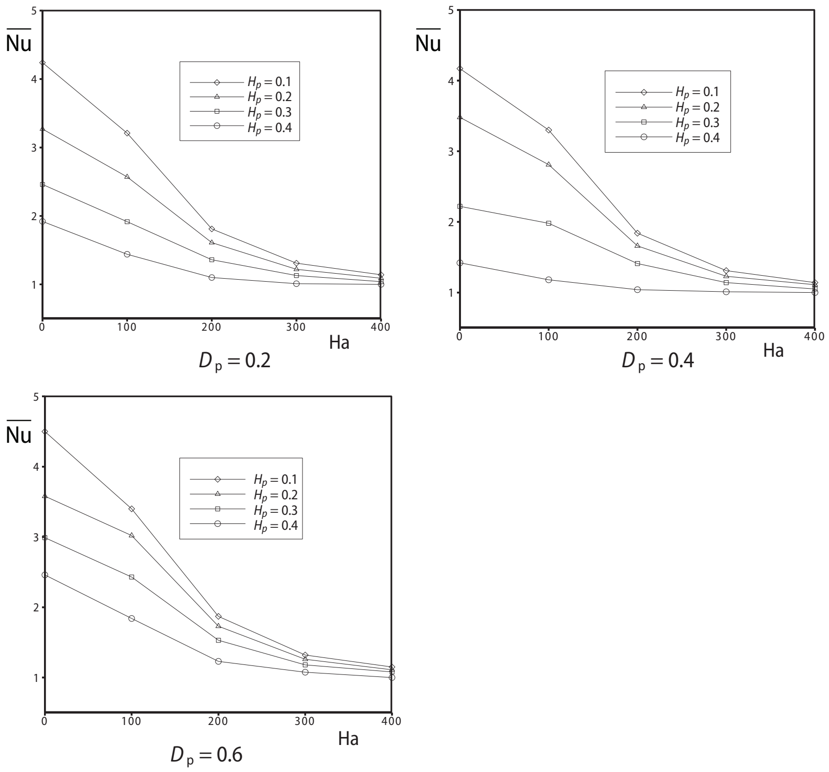

Figure 7. Variation of the mean Nusselt number with Hartmann number for Ra = 10^6 and different non-dimensional partition heights and positions: (a) D_p = 0.2, (b) D_p = 0.4, (c) D_p = 0.6

Flow field and heat transfer for Ra = 10^7

Figure 8 presents the isotherms and streamlines for Ra = 10^7, H_P = 0.2, $D_{P\,=}$ 0.2, and Hartmann numbers between 0 and 750.

In fig. 8(a) it is shown that at Ha = 0 in addition to secondary vortices that are formed inside the primary vortex, two counterclockwise vortices above the partitions are appeared. As Hartmann number increases these secondary vortices become small so that at high Hartmann numbers they are disappeared. It is evident from fig. 8(b) the thermal boundary-layer is formed near the hot and cold walls and the convection is dominant mechanism of heat transfer. As Hartmann number increases the stratification of isotherms at center of enclosure becomes lower and at high Hartmann numbers the isotherms will be vertical.

Figure 9 presents the isotherms and streamlines for Ra = 10^7, H_P = 0.2, D_P = 0.4, and Hartmann numbers between 0 and 750.

In fig. 9(a) it is seen that at Ha = 0 as well as the secondary vortices inside the main flow, two vortexes behind and above the partitions are formed. At Ha = 150 the vortices above the partitions become smaller and the other become bigger and the secondary vortices inside the primary vortex are disappeared.

Figure 9(b) indicates that effect of the partitions in blocking the fluid-flow and the reducing heat transfer is more than the other cases and the stratification of the isotherms at low Hartmann numbers is less so that at high Hartmann numbers the conduction mode is dominant in enclosure.

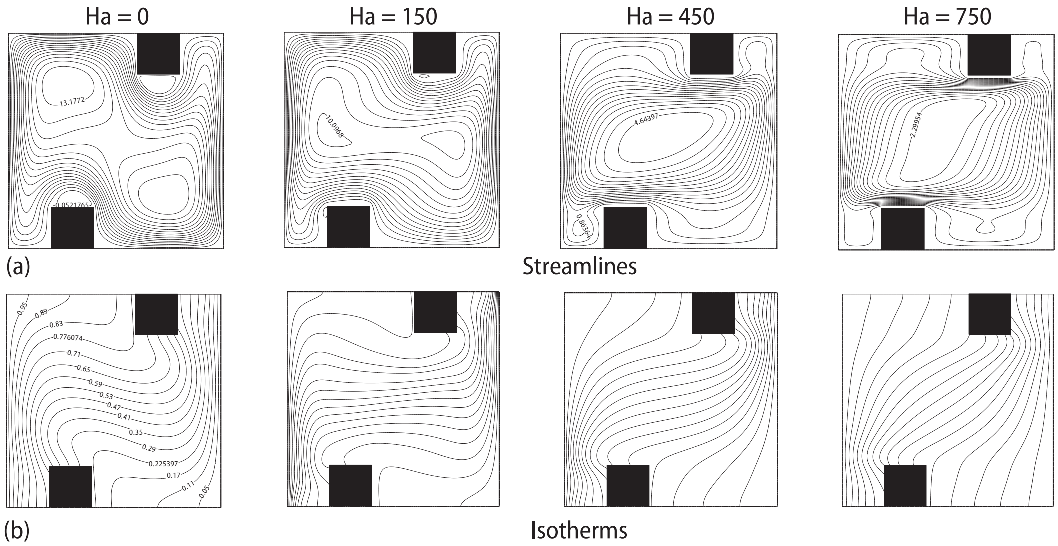

Figure 8. Streamlines (a) and isotherms (b) for D_p = 0.2, Ra = 10^7 and different Hartmann numbers

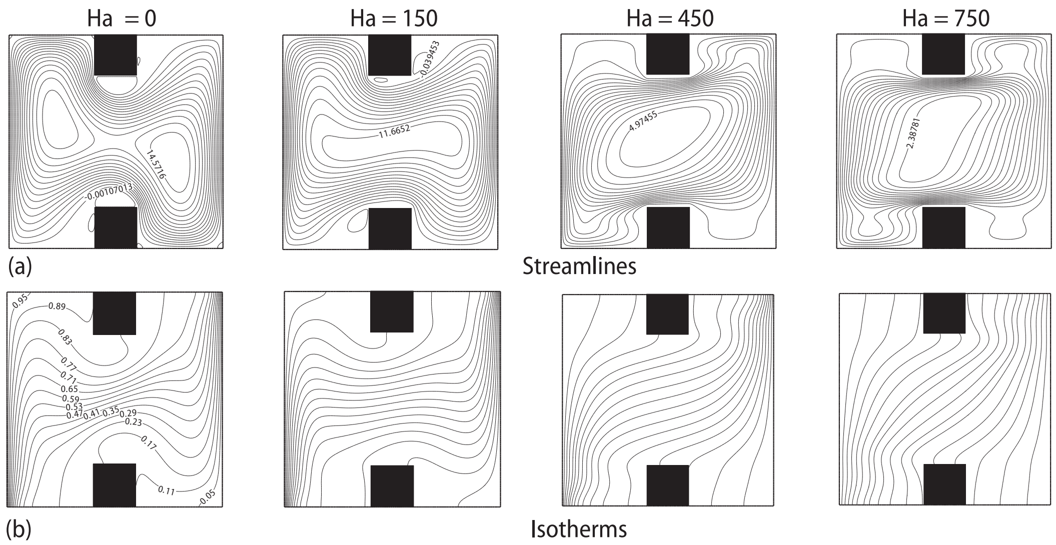

Figure 9. Streamlines (a) and isotherms (b) for D_p = 0.4, Ra = 10^7 and different Hartmann numbers

Figure 10 presents the isotherms and streamlines for Ra = 10^7, H_P = 0.2, D_P = 0.6, and Hartmann numbers between 0 and 750.

In fig. 10(a) it is depicted that when Ha = 0 in addition to primary flow two vortices behind the partitions are formed. At Ha = 150 these vortices become larger and weaker but as Hartmann number increases they are disappeared. At Ha = 900 two secondary vortices are seen in the primary vortex. It is evident from fig. 10(b) at Ha = 0 the thermal boundary-layer is formed near the hot and cold walls and as Hartmann number increases the stratification of isotherms and temperature gradient near the vertical walls reduces and at high Hartmann numbers the heat transfer occurs by conduction.

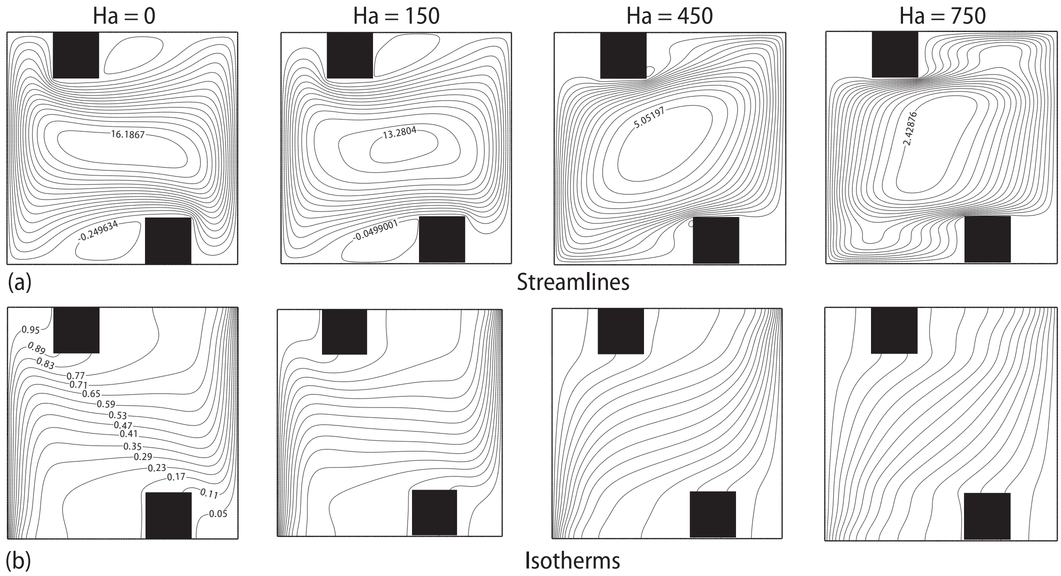

Figure 10. Streamlines (a) and isotherms (b) for D_p = 0.6, Ra = 10^7 and different Hartmann numbers

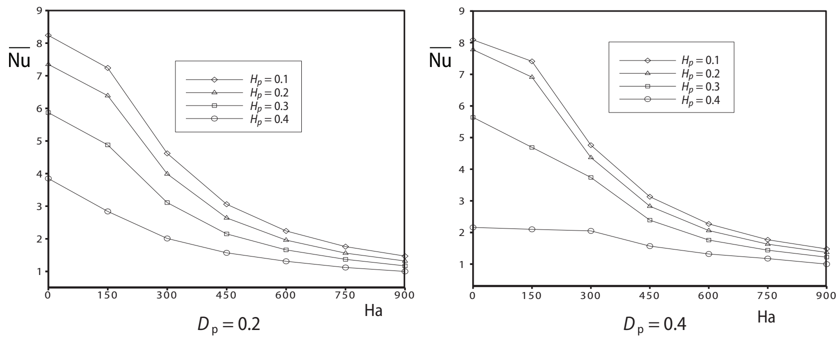

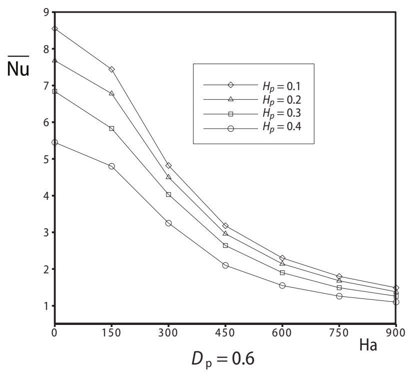

Figure 11. Variation of the mean Nusselt number with Hartmann number for Ra = 10^7 and different non-dimensional partition heights and positions: (a) D_p = 0.2, (b) D_p = 0.4, (c) D_p = 0.6

Figure 11 depicts the variation of the mean Nusselt number with Hartmann number versus several partition heights for D_p = 0.2, D_p = 0.4, D_p = 0.6, and Ra = 10^7.

It is observed that for D_p = 0.4 the variation of mean Nusselt number for different partition height is more different than the other cases. Also, it is observed that the Nusselt number at H_p = 0.4 is nearly half for D_p = 0.4 in comparison with the other cases. Because at Ra = 10^7

the advection is large and when $H_p = 0.4$ the flow blockage is the most and the enclosure is divided to two hot and cold zones, so the heat transfer is less than the other cases.

Conclusions

- Generally, it is observed that as Hartmann number and partitions height increase the mean Nusselt number decreases.
- For Ra = 10^6 in low Hartmann numbers deviation between Nusselt numbers for different H_p is high and with increasing the magnetic field strength this deviation decreases. Also, it is seen that at $D_p = 0.6$ the Nusselt number is maximum and as Hartmann number increases the Nusselt number tends to a constant number.
- For Ra = 10^7 it is observed that at $D_p = 0.4$ the variation of mean Nusselt number for different partition height is more different than the other cases. Also, it is observed that the Nusselt number at $H_p = 0.4$ is nearly half for $D_p = 0.4$ in comparison with the other cases.

Nomenclature

D_p – partition position
g – acceleration due to gravity
H – height of the cavity
H_p – partition height
K' – von Karman constant
k – thermal conductivity
$\underline{\mathrm{Nu}}$ – local Nusselt number
Nu – mean Nusselt number
P – pressure
Pr – Prandtl number
Ra – Rayleigh number
T – temperature
T^+ – wall function for temperature
u, v – velocity components
y_p – distance of a point from wall.

Greek Symbols

α – thermal diffusivity
β – coefficient of thermal expansion
ε – issipation rate
θ – dimensionless temperature
κ – turbulent energy
μ – dynamic viscosity
μ_t – urbulent viscosity
ν – kinematic viscosity
ρ – density

Subscripts

c – cold
f – fluid
h – hot
s – solid

Reference

[1] Rudraiah, N., *et al.*, Effect of a Magnetic Field on Free Convection in a Rectangular Cavity, *International Journal of Engineering Science*, *33* (1995), 8, pp. 1075-1084
[2] Al-Najem, N. M., *et al.*, Numerical Study of Laminar Natural Convection in Tilted Cavity with Transverse Magnetic Field, *International Journal of Numerical Methods for Heat Fluid Flow*, *8* (1998), Sept., pp. 651-672
[3] Bondareva, N. S., *et al.*, Magnetic Field Effect on the Unsteady Natural Convection in a Right-Angle Trapezoidal Cavity Filled with a Nanofluid, *International Journal of Numerical Methods for Heat Fluid Flow*, *25* (2015), Nov., pp. 1924-1946
[4] Sheremet, M. A., *et al.*, Magnetic Field Effect on the Unsteady Natural Convection in a Wavy-Walled Cavity Filled with a Nanofluid: Buongiorno's Mathematical Model, *Journal of the Taiwan Institute of Chemical Engineers*, *61* (2016), Apr., pp. 211-22
[5] Pirmohammadi, M., Ghassemi, M., Effect of Magnetic Field on Convection Heat Transfer Inside a Tilted Square Enclosure, *International Communications in Heat and Mass Transfer*, *36* (2009), 7, pp. 776-780
[6] Pirmohammadi, M., *et al.*, Numerical Study of Hydromagnetic Convection of an Electrically Conductive Fluid with Variable Properties inside an Enclosure, *IEEE Transactions on Plasma Science*, *39* (2011), 1, pp. 516-520
[7] Jalil, J. M., Al-Tae'y, K. A., The Effect of Nonuniform Magnetic Field on Natural Convection in an Enclosure, *Numerical Heat Transfer, Part A*, *51* (2007), 9, pp. 899-917

[8] Kakarantzas, S. C., *et al.*, Natural Convection of Liquid Metal in a Vertical Annulus with Lateral and Volumetric Heating in the Presence of a Horizontal Magnetic Field, *International Journal of Heat and Mass Transfer*, *54* (2011), 15-16, pp. 3347-3356
[9] Liu, X., *et al.*, Effects of Static Magnetic Fields on Thermal Fluctuations in the Melt of Industrial CZ-Si Crystal Growth, *Journal of Crystal Growth*, *360* (2012), Dec., pp. 38-42
[10] Kakarantzas, S. C.,*et al.*, Magnetohydrodynamic Natural Convection of Liquid Metal Between Coaxial Isothermal Cylinders due to Internal Heating, *Numerical Heat Transfer, Part A*, *65* (2014), 5, pp. 401-418
[11] Zhang, X., Zikanov, O., Two-Dimensional Turbulent Convection in a Toroidal Duct of a Liquid Metal Blanket, *Journal of. Fluid Mechanics, 779* (2015), Sept., pp. 36-52
[12] Sajjadi, H., Kefayati, G. H. R., MHD Turbulent and Laminar Natural Convection in a Square Cavity Utilizing Lattice Boltzmann Method, *Heat Transfer – Asian Research, 45* (2016), 8, pp. 795-814
[13] Enayati, H., *et al.*, Numerical Simulations of Transitional and Turbulent Natural Convection in Laterally Heated Cylindrical Enclosures for Crystal Growth, *Numerical Heat Transfer, Part A*, *70* (2016), 11, pp.1195-1212
[14] Versteeg, H., Malalaskera, W., *An Introduction to Computational Fluid Dynamics*, Longman Scientific & Technical, London, 1995
[15] Sarris, I. E., *et al.*, On the Limits of Validity of the Low Magnetic Reynolds Number Approximation in MHD Natural-Convection Heat Transfer, *Numerical Heat Transfer (Part B)*, *50* (2006), 2, pp. 157-180
[16] Heidary H., *et al.*, Magnetic Field Effect on Convective Heat Transfer in Corrugated Flow Channel, *Thermal Science, 21* (2017), 5, pp. 2105-2115
[17] Jayatilleke, C. L. V., The Influence of Prandtl Number and Surface Roughness on the Resistance of Laminar Sublayer to Momentum and Heat Transfer, *Heat and Mass Transfer, 1* (1966), 193
[18] Patankar, S. V., *Numerical Heat Transfer and Fluid Flow*, Hemisphere, Washington, DC, 1980

Paper submitted: November 1, 2017
Paper revised: February 4, 2018
Paper accepted: March 3, 2018